https://doi.org/10.5194/egusphere-2024-3252
Preprint. Discussion started: 6 December 2024

Quantifying transboundary transport flux of CO over the Tibetan Plateau: variabilities and drivers

Zhenda Sun [1)], Hao Yin [2)], Zhongfeng Pan[3)], Chongyang Li[1)], Xiao Lu [4)], Youwen Sun [1,5)*] and Cheng Liu [6,7,8,9)*]

(1 *School of Environmental Science and Optoelectronic Technology, University of Science and Technology of China, Hefei 230026, China*)

(2 *School of Energy and Environment, City University of Hong Kong, Hong Kong SAR, China*)

(3 *Institutes of Physical Science and Information Technology, Anhui University, Hefei 230601, China*)

(4 *School of Atmospheric Sciences, Sun Yat-Sen University, Zhuhai 519082, China*)

(5 *Key Laboratory of Environmental Optics and Technology, Anhui Institute of Optics and Fine Mechanics, HFIPS, Chinese Academy of Sciences, Hefei 230031, China*)

(6 *Department of Precision Machinery and Precision Instrumentation, University of Science and Technology of China, Hefei 230026, China*)

(7 *Center for Excellence in Regional Atmospheric Environment, Institute of Urban Environment, Chinese Academy of Sciences, Xiamen, 361021, China*)

(8 *Key Laboratory of Precision Scientific Instrumentation of Anhui Higher Education Institutes, University of Science and Technology of China, Hefei, 230026, China*)

(9 *Anhui Province Key Laboratory of Polar Environment and Global Change, USTC, Hefei, 230026, China*)

Correspondence: ywsun@aiofm.ac.cn; chliu81@ustc.edu.cn

Abstract:

The Tibetan Plateau significantly impacts regional and global climate systems due to its unique geographical location and complex environmental processes. This study investigates the variability and driving force of transboundary transport flux of carbon monoxide (CO) over the Tibetan Plateau from May 2018 to April 2024. The transport CO fluxes were calculated with a closed-loop integral method using the TROPOMI, ERA5, and GEOS-CF data products. The results show that the external influx and internal efflux of CO over the Tibetan Plateau in each year are relatively close and have similar seasonal characteristics. High levels of CO flux occur in late autumn to winter, and low levels occur in summer. In most cases, CO flux maximizes in November, December or January, and minimizes in July or August. The month to month variability during late autumn to winter is greater than that in summer. The Tibetan Plateau has experienced an increase of 0.65 t s^{-1} yr^{-1} in external influx, while the internal efflux has slightly decreased by -0.39 t s^{-1} yr^{-1}. The magnitude of the increase in external influx in the southwestern segment is greater than in the northeastern segment. Conversely, the magnitude of the decrease in internal efflux in the northeastern segment is greater than in the southwestern segment. The source attribution results reveal that the external input of CO into the Tibetan Plateau mainly comes from

https://doi.org/10.5194/egusphere-2024-3252
Preprint. Discussion started: 6 December 2024

South Asia. The increase in external influx of CO in recent years over the Tibetan Plateau are potentially linked to the rapid rise in CO concentrations from South Asia.

1 Introduction

The Tibetan Plateau, often referred to as the "Third Pole of the Earth", is characterized by its extensive snow, glaciers, permafrost, and seasonal frozen ground. Due to the complex interactions among atmospheric, cryospheric, hydrological, geological, and environmental processes, this region profoundly impacts global climate and water cycle systems. The Tibetan Plateau plays a crucial role in the global climate system and serves as a critical indicator of regional and global climate change (Qian et al., 2011; Li et al., 2017; Bibi et al., 2018; Gao et al., 2019). This plateau and its surrounding regions experience various atmospheric circulation patterns, including the Indian summer monsoon, winter westerlies, and the East Asian monsoon (Yao et al., 2012; Chen et al., 2020). These circulation patterns are essential in shaping regional climate and pollutant transport. In particular, the southwestern Tibetan Plateau is influenced by the South Asian monsoon. During summer, the intensified monsoon transports warm, moist air masses and pollutants, such as aerosols and particulate matter, from the South Asian subcontinent to the Tibetan Plateau. Owing to the uplift effect of the plateau's topography, these airflows descend into the southern and southwestern regions after crossing the Himalayas, delivering rainfall and accumulating pollutants. Conversely, the northeastern Tibetan Plateau are impacted by the East Asian monsoon. In winter, cold air from Central and Northern Asia flows into the plateau, carrying pollutants from these areas. In summer, the East Asian monsoon brings moist air and pollutants from the East Asian coast into the eastern Tibetan Plateau, affecting local air quality (Ramanathan et al., 2005; Xu et al., 2009; Kaspari et al., 2011; Qian et al., 2011; Lüthi et al., 2015; Cong et al., 2015; Zhang et al., 2015; Wang et al., 2019; Wu et al., 2020; Li et al., 2021; Sun et al., 2021). Surrounding the Tibetan Plateau, densely populated Eurasian countries are experiencing rapid economic development, leading to increased emissions of air pollutants. Consequently, these regions have become some of the most polluted areas globally, and the pollutants can be transported over long distances to the Tibetan Plateau via the Asian monsoon and westerly circulation (Lawrence and Lelieveld, 2010). In addition to the rising industrial and agricultural emissions within the Tibetan Plateau, these external pollutants can also significantly impact its ecosystem and climate (Ji et al., 2015; Sun et al., 2021; Yin et al., 2022).

Carbon monoxide (CO) is one of the most significant atmospheric pollutants, primarily resulting from incomplete combustion of fossil fuels, biomass burning, and the oxidation of methane and non-methane hydrocarbons. This pollutant can indirectly exacerbate global warming by participating in the formation and reactions of other greenhouse gases in the atmosphere. CO is predominantly removed from the atmosphere through reactions with hydroxyl radicals (OH) (Holloway et al., 2000; Heald et al., 2003; Luo et al., 2013; Martínez-Alonso et al., 2020). With a lifetime ranging from several weeks to months, CO can persist in the atmosphere for extended periods, undergoing both horizontal and vertical transport. Consequently, CO is frequently employed as a tracer for studying pollutant transport dynamics (Holloway et al., 2000; Gloudemans et al., 2006; Jeong and Hong, 2021). Given its unique chemical properties and significant climatic effects, studying CO flux, variability, and driving factors offers valuable insights into the atmospheric conditions over the Tibetan Plateau. Furthermore, CO sources may

https://doi.org/10.5194/egusphere-2024-3252
Preprint. Discussion started: 6 December 2024

vary across different regions, understanding their contributions to the variability of CO flux over the Tibetan Plateau is essential for developing effective management strategies.

To investigate transboundary transport flux of CO over the Tibetan Plateau, this study employs a comprehensive array of data products, including TROPOMI, ERA5, and GEOS-CF. By integrating a closed-loop integral method with a regression model, we elaborate a top-down approach based on satellite remote sensing to estimate CO flux across the Tibetan Plateau. This quantitative analysis encompasses transport flux of CO along the Tibetan Plateau boundary (hereafter the closed-loop flux), spanning from the surface at 1000 hPa to the stratosphere at 50 hPa, over a nearly six-year time series from May 2018 to April 2024. Our analysis emphasizes seasonal and inter-annual variabilities of the closed-loop CO flux. We further split the closed-loop CO flux into sub-fluxes arising from southwestern and northeastern segments, enabling us to quantify the impacts of surrounding areas on the Tibetan Plateau. This study aims to elucidate the spatiotemporal variabilities and the driving forces of the CO transport flux over the Tibetan Plateau, thereby providing scientific evidence for a deeper understanding of the Tibetan Plateau's role in global climate and environmental dynamics.

In the subsequent section, we present an overview of the Tibetan Plateau territory, providing a concise description of the dataset utilized, along with the methodologies employed for the closed-loop integral calculation and trend regression model. The third section delves into the spatiotemporal dynamics of the CO total column and transport flux over the Tibetan Plateau, highlighting the trend fitting outcomes. The fourth section elucidates the driving forces behind the variability of transboundary transport CO flux. The study culminates in the fifth section with a synthesis of our findings and conclusions.

2 Methodology and dataset

This section introduces geographical description of the Tibetan Plateau, the closed-loop integral method used to derive external influx and internal efflux of CO, the regression model used for trend analysis and the dataset involved.

2.1 Geographical description of the Tibetan Plateau

We have conducted an analysis of both the external influx and internal efflux of CO across the Tibetan Plateau. The external influx refers to the quantity of CO that is transported from regions outside the Tibetan Plateau into its boundaries. Conversely, the internal efflux denotes the amount of CO that is generated within the Tibetan Plateau and dispersed to areas beyond its confines. As shown in Figure 1, we bifurcated the Tibetan Plateau's geographical boundary into two segments. The first segment encompasses the southwestern Tibetan Plateau, which is significantly influenced by the South Asian monsoon. The substantial topographic rise in this area intensifies the monsoon's impact (Huang et al., 2023). The second segment is situated in the northeastern Tibetan Plateau, where the westerlies and the East Asian monsoon play a pivotal role. There is a marked geographical disparity between these two segments.

For comparison, we annotate the adjacent regions around the Tibetan Plateau. We categorize these regions into three broad zones: the western, central, and eastern zones. The western zone predominantly comprises Himachal Pradesh, Uttarakhand, and Ladakh. The central zone is characterized by Nepal, Sikkim, and Bhutan, while the eastern zone includes Assam, Sagaing, and Kachin State, among others. A visual representation of these regional demarcations is presented in

https://doi.org/10.5194/egusphere-2024-3252
Preprint. Discussion started: 6 December 2024

Figure 1.

2.2 Dataset description

We utilize a comprehensive dataset encompassing the total column of CO measured by the TROPOMI instrument, the vertical profile of CO from the GEOS-CF system, meteorological data extracted from the ERA5 reanalysis, and atmospheric air-mass simulated by the GEOS-Chem model.

TROPOMI is a push broom imaging spectrometer on the ESA Sentinel-5 platform, providing daily global coverage of CO total column at 13:30 local time (LT) (Veefkind et al., 2012; Landgraf et al., 2020). We used TROPOMI Level 2 CO and filtered the TROPOMI data according to the method of Landgraf et al. (2020), i.e., we removed all pixels with a TROPOMI quality mark below 0.5, leaving only data with no clouds or only low-altitude clouds. For convenience of calculation, we resampled the CO data product in space and time to match the spatiotemporal resolution of the meteorological field.

ERA5 is the fifth generation of atmospheric reanalysis dataset for global climate from ECMWF (European Centre for Medium-Range Weather Forecasts). It provides hourly global atmospheric, land surface and ocean wave estimates since 1950 and is produced by the Copernicus Climate Change Service (C3S) of ECMWF (Hersbach et al., 2020). We extracted the wind vectors that coincident with the Sentinel-5's overpass time with a vertical resolution of 50 hPa from 50 hPa to 900 hPa and 25 hPa from 900 hPa to 1000 hPa.

Since measurement-based CO profile is not available, the vertical CO profile from the GEOS-CF system is used to correct vertically non-uniform distribution of CO concentration and wind field. The GEOS-CF system is a near-real-time high resolution (0.25° × 0.25°) global 3D coupled chemical and meteorological modeling system developed by NASA's Global Modeling and Assimilation Office (GMAO) (Keller et al., 2021). Since 2018, GEOS-CF has provided global CO vertical profiles at 23 pressure levels (from 1000 to 10 hPa) on an hourly basis.

The air-mass dataset used for calculating CO flux comes from the simulations of GEOS-Chem model version 12.2.1 (https://doi.org/10.5281/zenodo.2580198, International GEOS-Chem Community, 2019) (Long et al., 2015). The model is driven by assimilated meteorological data obtained from the Goddard Earth Observing System (GEOS) of NASA's Global Modeling and Assimilation Office (GMAO) (Bey et al., 2001). The GEOS-FP dataset has a horizontal resolution of 0.25 ° latitude × 0.3125 ° longitude and includes 47 vertical levels from the surface to 0.01 hPa. Surface meteorological variables and planetary boundary layer height (PBLH) are provided with a 1-hour interval. We used a nested grid version of GEOS-Chem with a horizontal resolution covering the East Asia region (70–140 ° E, 15–55 ° N), with boundary conditions derived from a global simulation at a resolution of 2 ° latitude × 2.5 ° longitude (Lee and Park, 2022).

2.3 The closed-loop integral method for CO flux calculation

We use the closed-loop integral method from Shaiganfar et al. (2017) to calculate the CO flux along the Tibetan Plateau boundary. With this closed-loop integral method, the external influx ($Flux, in$) and internal efflux ($Flux, out$) of CO across the Tibetan Plateau can be calculated as equations (1) and (2), respectively. The calculation methodology is illustrated in Figure 1.

https://doi.org/10.5194/egusphere-2024-3252
Preprint. Discussion started: 6 December 2024

$$Flux,in \approx -\sum VCD(S_i) \cdot \omega_i \cdot \cos\beta_i \cdot \Delta S_i \quad , \quad \beta_i > 90^{\circ} \quad (1)$$

$$Flux,out \approx \sum VCD(S_i) \cdot \omega_i \cdot \cos\beta_i \cdot \Delta S_i \quad , \quad \beta_i < 90^{\circ} \quad (2)$$

$$Flux,net = Flux,in - Flux,out \quad (3)$$

Where $VCD(S_i)$ represents CO total column locates at the path S_i, which represents the i^{th} segment of the path S. β_i is the angle between the wind field vector ω and the boundary normal vector n. If $\beta_i > 90^{\circ}$, it indicates an external influx, representing the quantity of CO that is transported from regions outside the Tibetan Plateau into its boundaries. if $\beta_i < 90^{\circ}$, it indicates an internal efflux, representing the amount of CO that is generated within the Tibetan Plateau but dispersed to areas beyond its confines. ΔS_i represents the integration step size. *Flux, net* calculated as the difference between *Flux,in* and *Flux,out* represent the net CO flux across the Tibetan Plateau boundary. If $Flux,net > 0$, it means that the portion transported from outside regions into Tibetan Plateau is larger than the portion transported from Tibetan Plateau to the outside regions, and vice versa for $Flux,net < 0$.

2.4 Wind field correction and uncertainty

ERA5 provides wind field components u and v along with their uncertainties σ_u and σ_v. Therefore, the wind speed ω_{spd} and wind direction w_{dir} can be calculated as equation (4),

$$\omega_{spd} = \sqrt{u^2 + v^2}, \quad w_{dir} = 180 + \frac{180}{\pi} atan2(u, v) \quad (4)$$

The uncertainty in the wind field can be calculated using the error propagation formulas (5) and (6),

$$\sigma_{wspd} = \sqrt{\sum_i [(\frac{\partial w_{spd(zi)}}{\partial u(zi)} \times \sigma_{u(zi)})^2 + (\frac{\partial w_{spd}(zi)}{\partial v(zi)} \times \sigma_{v(zi)})^2]} \quad (5)$$

$$\sigma_{wdir} = \sqrt{\sum_i [((\frac{\partial w_{dir}(zi)}{\partial u(zi)} \times \sigma_{u(zi)})^2 + (\frac{\partial w_{dir(zi)}}{\partial v(zi)} \times \sigma_{v(zi)})^2]} \quad (6)$$

Where σ_{wspd} and σ_{wdir} are the uncertainties in wind speed and wind direction, respectively. $\sigma_{u(zi)}$ and $\sigma_{v(zi)}$ are the uncertainties in $u(zi)$ and $v(zi)$, $\frac{\partial w_{spd(zi)}}{\partial u(zi)}$ and $\frac{\partial w_{spd}(zi)}{\partial v(zi)}$ are the partial derivatives of $w_{spd(zi)}$ with respect to $u(zi)$ and $v(zi)$, $\frac{\partial w_{dir}(zi)}{\partial u(zi)}$ and $\frac{\partial w_{dir(zi)}}{\partial v(zi)}$ are the partial derivatives of $w_{dir}(zi)$ with respect to $u(zi)$ and $v(zi)$, respectively. The zi represents the height of the wind field.

Since CO concentration and wind field are distributed non-uniformly along with the vertical height, a vertically averaged wind field is needed for flux calculation to minimize errors caused by these non-uniformities. In order to do so, we first convert the volume mixing ratio (VMR) of CO at each altitude into mass concentration (the product of vertical profile and atmospheric air mass) via equation (7). We then take it as the weighting function to correct the original wind field via equation (8) (Shaiganfar et al., 2017; Huang et al., 2020). Meanwhile, we calculate the uncertainty in the wind field following the method of Huang et al. (2020).

$$\tau_j(z_j) = \frac{x_j(z_j) \cdot Airmass_j(z_j)}{\sum_i x_j(z_j) \cdot Airmass_j(z_j)} \quad (7)$$

$$\omega_{j,avg} = \sum_i \omega(z_i) \cdot \tau_j(z_j), \quad \theta_{j,avg} = \sum_i \theta(z_i) \cdot \tau_j(z_j) \quad (8)$$

https://doi.org/10.5194/egusphere-2024-3252
Preprint. Discussion started: 6 December 2024

$$\sigma_{\omega z} = \sqrt{\sum_i [\tau_j(\omega_{j,avg} - \omega(z_i))]^2}, \sigma_{\theta z} = \sqrt{\sum_i [\tau_j(\theta_{j,avg} - \theta(z_i))]^2} \quad (9)$$

Where $\omega(z_i)$, $x_j(z_j)$, and $Airmass_j(z_j)$ represent the wind field vector, CO VMR concentration, and air mass at height z_j along the j segment of the integration path, respectively. $\omega_{j,avg}$ is the weighting averaged wind field along the j segment of the integration path, and $\sigma_{\omega z}$ and $\sigma_{\theta z}$ are the uncertainties in the corrected wind field and wind direction, respectively.

2.6 Regression model for trend analysis

We establish a regression model expressed as equations (10) and (11) to simulate the seasonal and inter-annual variabilities of transboundary transport CO flux along the Tibetan Plateau boundary. This model consists of a third-order Fourier series and a linear function. We refer to Sun et al. (2021) for detailed description of its resampling methodology.

$$Y^{org}(t) = Y^{mod}(t) + \varepsilon(t) \quad (10)$$

$$Y^{mod}(t) = A_0 + A_1 t + A_2 \cos\left(\frac{2\pi t}{365}\right) + A_3 \sin\left(\frac{2\pi t}{365}\right) + A_4 \cos\left(\frac{4\pi t}{365}\right) + A_5 \sin\left(\frac{4\pi t}{365}\right) \quad (11)$$

$$d\% = \frac{Y^{org}(t) - Y^{mod}(t)}{Y^{mod}(t)} \times 100 \quad (12)$$

where $Y^{org}(t)$ and $Y^{mod}(t)$ are the original and the fitted time series of CO flux, respectively. A_0 is the intercept, A_1 is the annual growth rate, and t represents the number of days since May 2018. The $\varepsilon(t)$ is the residual between the original and the fitted results. The coefficients $A_2 - A_5$ describe the seasonal cycle and A_1/A_0 is the inter-annual trend. Deviations of CO fluxes from their average seasonal values, known as seasonal enhancements, are calculated according to Equation (12).

3 Variability of CO total column and transboundary transport flux

3.1 Variability of CO total column

We average the CO total column along the Tibetan Plateau boundary and investigate its daily, seasonal and inter-annual variabilities. The results show that the daily mean CO total column ranges from 7.75×10^{17} molec cm^{-2} to 15.61×10^{17} molec cm^{-2}, while the seasonal mean ranges from 10.06×10^{17} molec cm^{-2} to 12.01×10^{17} molec cm^{-2}. As shown in Figure 2, high levels of CO total column in all seasons are observed in the southeastern segment of the Tibetan Plateau boundary, which is adjacent to southeastern Asia.

We employ the regression model to fit the CO total columns averaged along the closed-loop, the southwestern, and the northeastern segments of the Tibetan Plateau boundary. The fitting results in Figure 3 show that the model is capable of accurately capturing and replicating the seasonal and inter-annual variabilities of CO total column averaged using all the three manners. The correlation coefficient (r) achieved are 0.84, 0.90, and 0.75, while the root mean square error ($RMSE$) is 0.54×10^{17} molec cm^{-2}, 0.41×10^{17} molec cm^{-2}, and 0.76×10^{17} molec cm^{-2} for the closed-loop, the southwestern, and the northeastern segments, respectively. Satellite observations and the fitted results show distinct seasonal characteristics. Elevated levels of CO total column are observed along the closed-loop, northeastern, and southwestern segments from late spring to summer, while lower levels occur during autumn and winter. The closed-loop, southwestern, and northeastern segments all exhibit a bimodal seasonal cycle. The closed-loop and southwestern segment have a pronounced peak in late spring and a minor peak in early autumn, whereas the northeastern segment has a minor peak in late spring and a pronounced peak in early autumn. Notably, significant fluctuations in the CO total column averaged along the closed-loop, southwestern, and northeastern segments occur in autumn and winter, with more substantial fluctuations in autumn than in winter. Over the past six years, the CO total column averaged along the closed-loop, southwestern, and northeastern segments have shown an upward annual trends of 0.68×10^{15} molec cm^{-2} yr^{-1}, 0.55×10^{15} molec cm^{-2} yr^{-1}, and 0.78×10^{15} molec cm^{-2} yr^{-1}, respectively.

3.2 Variability of transboundary transport CO flux

Seasonal cycles of the external influx and internal efflux of CO across the closed-loop, the southwestern and northeastern segments of the Tibetan Plateau from May 2018 to April 2024 are shown in Figure 4. Summary of the corresponding statistics are tabulated in Table 1. The results show that the external influx and internal efflux of CO across the closed-loop, the southwestern, northeastern segments in each year are relatively close and have similar seasonal characteristics. High levels of CO flux occur in late autumn to winter, and low levels occur in summer. In most cases, CO flux maximizes in November, December or January, and minimizes in July or August. The month to month variability during late autumn to winter is greater than that in summer. For the closed-loop of the Tibetan Plateau, the CO external influx varies between 7.90t s^{-1} - 32.73t s^{-1} and the internal efflux varies between 7.84 t s^{-1} - 29.61 t s^{-1}. In comparison, the external influx in the southwestern segment fluctuates between 3.12 t s^{-1} and 20.89 t s^{-1}, while the internal efflux ranges from 1.15 t s^{-1} to 8.86 t s^{-1}. In the northeastern segment, the external influx varies between 3.42 t s^{-1} and 11.84 t s^{-1}, and the internal efflux spans from 5.47 t s^{-1} to 22.69 t s^{-1} (Table 1).

We applied an inter-annual regression model to fit the external influx, internal efflux and net flux of CO averaged along the closed-loop, southwestern and northeastern segments of the Tibetan Plateau. The fitting results in Figure 5 show that the model is capable of accurately capturing and replicating the seasonal and inter-annual variabilities of all kinds of fluxes, yielding high correlation coefficients (*r*) and low root mean square errors (*RMSE*). For the closed-loop CO flux, the external influx and net flux show slight positive trends, with inter-annual growth rates of 0.65 t s^{-1} yr^{-1} and 1.03 t s^{-1} yr^{-1}, respectively. In contrast, the internal efflux displays a slight negative trend of -0.39 t s^{-1} yr^{-1}. In the southwestern segment, the external influx and internal efflux exhibit similar variabilities, with annual mean values of 11.76 t s^{-1} and 4.41 t s^{-1}, respectively. The annual growth rates for external influx and internal efflux are 0.52 t s^{-1} yr^{-1} and -0.06 t s^{-1} yr^{-1}, respectively. In comparison, the external influx and internal efflux in the northeastern segment exhibit notable differences, with average values of 5.94 t s^{-1} and 13.17 t s^{-1}, and annual growth rates of 0.15 t s^{-1} yr^{-1} and -0.28 t s^{-1} yr^{-1}, respectively. The annual growth rates for net fluxes in the southwestern and northeastern segments are 0.59 t s^{-1} yr^{-1} and 0.42 t s^{-1} yr^{-1}, respectively.

This suggests that in recent years, the Tibetan Plateau has experienced an increase in external influx, while the internal efflux has slightly decreased. The magnitude of the increase in external influx in the southwestern segment is greater than in the northeastern segment. Conversely, the magnitude of the decrease in internal efflux in the northeastern segment is greater than in the southwestern segment.

3.3 Uncertainty of CO flux calculation

From May 2018 to April 2024, the external influx and internal efflux of CO averaged along the Tibetan Plateau were 17.70 t s^{-1} and 17.56 t s^{-1}, respectively, resulting in a net influx of 0.13 t s^{-1}. These estimates are based on TROPOMI overpasses (13:30 local time (LT)). Extrapolating to a full year, the external influx, internal efflux, and net influx are estimated to be 558.19 Tg yr^{-1}, 553.77 Tg yr^{-1}, and 4.10 Tg yr^{-1}, respectively. These values are comparable to CO emission estimated by Borsdorff et al. (2020) for Mexico and Leguijt et al. (2023) for African cities (Borsdorff et al., 2020; Leguijt et al., 2023).

The complex terrain of Tibetan Plateau, with its significant fluctuations in elevation and ground albedo, coupled with the variable mixture of the Asian monsoon and local valley winds, greatly increases the uncertainty of calculating CO flux over the Tibetan Plateau. TROPOMI-based CO flux calculation over the Tibetan Plateau are influenced by various factors (Shaiganfar et al., 2011; Shaiganfar et al., 2017; Tan et al., 2019; Huang et al., 2020). Here we identify two primary sources of uncertainty: CO total column and the closed-loop wind field.

From May 2018 to April 2024, daily CO total column over the Tibetan Plateau varied from 4.02×10^{17} molec cm^{-2} to 64.43×10^{17} molec cm^{-2}. The averaged standard deviation varied from 0.16×10^{17} molec cm^{-2} to 3.46×10^{17} molec cm^{-2}, corresponding to error margins from 0.81% to 17.89%. The average error in CO total column along the Tibetan Plateau's closed-loop was 4.27%.

Wind speed and direction uncertainties significantly affect CO flux calculations. The Tibetan Plateau's complex terrain exacerbates wind variability. Using formulas (5) and (6), and (9) in Section 2.3, we calculated the uncertainties from the corrected wind field across 22 levels from 1000 hPa to 50 hPa. The averaged wind speed and direction uncertainties were 3.39 m s^{-1} and 54.55°, respectively. Wind speed uncertainty exhibited clear seasonal fluctuations. In spring (MAM), uncertainties ranged from 0.65 to 0.84 m s^{-1}, while summer (JJA) saw a wider range of 0.90 to 1.15 m s^{-1}. The lowest uncertainties were observed in autumn (SON), ranging from 0.53 to 0.65 m s^{-1}. In winter (DJF), uncertainty values were slightly higher, between 0.65 and 0.71 m s^{-1}. Wind direction uncertainty also varied seasonally, with values between 18.10° and 26.41° in spring, increasing to 24.17° to 34.09° in summer. Autumn presented the lowest directional uncertainty, ranging from 16.50° to 20.62°, while winter values were comparable to spring, at 19.07° to 23.91° (Table 2).

The average uncertainties for the corrected wind speed and direction were 0.78 m s^{-1} and 22.15° . In calculation of the closed-loop CO flux, considering only the uncertainty in wind speed results in an average error of 6.99% in CO flux, while accounting solely for wind direction uncertainty leads to an average error of 11.03%. The total error induced by both the wind field and CO total column can be calculated using the error propagation equation. The uncertainty in CO flux caused by these factors amounts to 13.81%.

4 Factors driving the variability of transboundary transport CO flux

4.1 Differences between southwestern and northeastern segments

For the closed-loop flux, both external influx and internal efflux exhibit significant fluctuations in winter from 2020 to 2023, followed by a rapid decline. Although the net flux also exhibited considerable fluctuations during this period, its seasonal variability was less pronounced compared to the external influx and internal efflux. The net flux is positive from January to May and in August and December, but turns negative in June, July, and from September to November. Specifically, the external influx in the southwestern segment consistently exceeds the internal

https://doi.org/10.5194/egusphere-2024-3252
Preprint. Discussion started: 6 December 2024

efflux, whereas in the northeastern segment, the external influx is lower than the internal efflux. Furthermore, the external influx in the southwestern segment closely resembles that of the internal efflux in the northeastern segment, particularly during summer and early autumn when the rates of decline and increase are most pronounced. Conversely, during winter and early spring, the internal efflux in the southwestern segment aligns closely with the external influx in the northeastern segment. Additionally, in summer, the external influx in the northeastern segment surpasses the internal efflux in the southwestern segment.

In the southwestern segment, a significant increase in flux is noted during autumn, followed by a marked decline in late winter. The net flux variations are more intricate, yet they generally remain positive. The averaged net CO flux is recorded at 7.36 t s^{-1}, with an annual growth rate of -0.59 t s^{-1} yr^{-1}, typically exhibiting low values during the summer. Notably, from December to June in each year, the net flux experiences three distinct peaks. The first peak is observed during late autumn and winter, attributed to increased burning activities, such as winter heating and agricultural burning, alongside the enhanced transport of strong westerly airflow. These conditions contribute to elevated flux levels. Furthermore, cold winter temperatures inhibit the diffusion and dilution of pollutants, facilitating their accumulation in localized areas (Kunhikrishnan et al., 2004). The second peak occurs in spring, influenced by several factors, including rising temperatures, melting ice and snow, and the onset of plant growth. These conditions promote the release of pollutants into the atmosphere (Assessment, 2004; Hung et al., 2022). Additionally, frequent climate fluctuations may destabilize the emission and transport processes of these pollutants. The third peak is observed around June, coinciding with the strengthening of the South Asian monsoon. This seasonal shift brings increased moisture and airflow, which aids in diluting pollutants and facilitating their transport over long distances (Yu et al., 2017; Bian et al., 2020; Huang et al., 2023).

In the northeastern segment, the external influx peaks in both summer and winter. In winter, there is a marked increase in external influx, followed by two declines in early and late spring. This behavior is likely influenced by the dynamics of the East Asian monsoon across different seasons and varying intensities of burning activities throughout the year. The internal efflux displays a more complex pattern, featuring three peaks and subsequent declines in winter, March, and June, which correspond to the three peaks of net flux observed in the southwestern segment. Similarly, the net flux variabilities in the northeastern segment are quite intricate. The average net CO flux is -7.23 t s^{-1}, with an annual growth rate of -0.42 t s^{-1} yr^{-1}. The peak and trough values occur around autumn, specifically in late autumn to early winter for peaks and late autumn for troughs. This downward trend mirrors that of the internal efflux. Additionally, we observed that: (1) The CO flux transported through the southwestern segment into the Tibetan Plateau, along with its annual growth rate over the past six years, accounted for approximately 66.44% and 77.61% of the total CO flux within the Tibetan Plateau. This indicates that the external influx to the Tibetan Plateau and its changing trend are predominantly influenced by the southwestern segment. While CO transported through the southwestern segment into the Tibetan Plateau is on the rise, the internal efflux transported through the northeastern segment is experiencing a decline; (2) Around June each year, we observe minor seasonal peaks in the external influx and net flux across the southwestern segment, as well as in the internal efflux across the northeastern segment. This phenomenon may result from the combined effects of atmospheric circulation and the South Asian summer monsoon mechanism. The atmospheric flow prior to the onset of the South Asian

https://doi.org/10.5194/egusphere-2024-3252
Preprint. Discussion started: 6 December 2024

monsoon transports pollutants such as CO from South Asia to the Tibetan Plateau, leading to increased CO concentrations and fluxes in the region (Yu et al., 2017; Huang et al., 2023). This seasonal peak also highlights the intricate interactions between atmospheric circulation and the monsoon system in South Asia during the pollutant transmission process. (3) The southwestern segment exhibits distinct pollutant transport differences compared to the northeastern segment. For example, the averaged external influx across the southwestern segment reaches as high as 11.99 t s^{-1}, while the averaged internal efflux across the northeastern segment is only 4.60 t s^{-1}. This is primarily attributed to a higher level of rapid industrialization and urbanization in Southeast Asia than in Tibetan Plateau, resulting in higher pollutant emissions (including CO) in the region.

Eastern China is predominantly downwind of the Tibetan Plateau, where the wind flow and atmospheric stability in the upper atmosphere predispose the eastern region to act as a receiving area for pollutants from the Tibetan Plateau. The Tibetan Plateau functions as a high-altitude natural barrier, effectively limiting the in-depth spread of pollutants (Ji et al., 2015). However, the rapid industrialization and urbanization in East China have led to high local pollutant emissions. Influenced by atmospheric circulation patterns and complex topography, East China experiences strong convection and large-scale circulatory systems. While most pollutants are recirculated and deposited within the region, significant transport occurs towards South Korea, Japan, and the North Pacific. A smaller fraction may also reach the eastern edge of the Tibetan Plateau. (Zhang et al., 2015; Yan and Bian, 2015).

4.2 Spatiotemporal distribution of CO

We have analyzed spatiotemporal distribution of CO total column from May 2018 to April 2024 over the Tibetan Plateau and its surrounding regions. CO total columns were averaged on both annual and seasonal timescales. Specifically, we estimated the average of CO total column for winter (December to February), the pre-monsoon period (March to May), the monsoon period (June to September), and the post-monsoon period (October to November). Seasonal variations were assessed by subtracting the mean annual CO total column from their seasonal averages. The resulting data are presented in Figures 6. Additionally, we analyzed the six-year average spatial distribution and correlation of CO total column concentrations across the Indian states of Himachal Pradesh, Uttarakhand, and Ladakh, as well as Nepal and Assam. The corresponding results are presented in Figure 7.

The results indicate that CO concentrations over the Tibetan Plateau are consistently lower than those in South Asia throughout the year. CO levels in South Asia are particularly elevated, especially during winter and spring, when the disparity is most pronounced. In summer, CO over the Tibetan Plateau disperses across a broader area. Notably, we observed that CO concentrations over the Tibetan Plateau are significantly higher than the annual average during the monsoon season. Specifically, the average CO concentration over the Tibetan Plateau increased by 0.90×10^{17} molec cm^{-2} compared to the annual mean, whereas in India and Nepal, CO concentrations decreased by -2.62×10^{17} molec cm^{-2} and -0.36×10^{17} molec cm^{-2}, respectively. These findings suggest that CO pollutants from South Asia are transported into the Tibetan Plateau during the South Asian monsoon. Over the past six years, the CO total column in northwestern India, Nepal, and Assam has exhibited relatively high growth rates, with annual increases of 1.10×10^{15} molec cm^{-2} yr^{-1}, 1.69×10^{15} molec cm^{-2} yr^{-1}, and 1.64×10^{15} molec cm^{-2} yr^{-1}, respectively.

https://doi.org/10.5194/egusphere-2024-3252
Preprint. Discussion started: 6 December 2024

The increase of CO over the Tibetan Plateau during summer may be influenced by CO influx driven by the South Asian monsoon, as well as various meteorological factors. High temperatures and intense solar radiation in summer raise the atmospheric mixing layer height, facilitating the easier dispersion of pollutants in the atmosphere (Yang et al., 2004; Huang et al., 2023). Additionally, summer precipitation and wind speed affect the spatial distribution and transport pathways of pollutants. Elevated temperatures and strong convective conditions enhance vertical mixing and horizontal transport, resulting in more extensive and rapid diffusion of pollutants across the Tibetan Plateau (Zhang et al., 2020; Sun et al., 2021).

During winter and spring, CO concentrations rise significantly in South Asian regions, including Nepal, Bhutan, Assam in India, and parts of Myanmar. This increase is likely driven by intensified human activities, such as biomass burning, which is common in these areas during these seasons for heating and agricultural waste disposal, leading to substantial CO emissions. The southern Tibetan region, bordering northern Assam, serves as a key pathway for pollutant transport due to its distinct plain topography. Studies have confirmed that persistent organic pollutants, HCHO, and other contaminants are transported along the Yarlung Tsangpo River valley into the Tibetan Plateau (Sheng et al., 2013; Xu et al., 2024). TROPOMI remote sensing data further show that CO pollutants infiltrate the Tibetan Plateau through this region.

Despite the varying geographical, climatic conditions, and emission sources in these regions, the changes in CO concentrations are interrelated. CO levels tend to be lower in high-altitude areas, such as Himachal Pradesh, Uttarakhand, and Ladakh. Nepal, particularly the Kathmandu Valley, faces unique geographic and climatic challenges due to its dense population and concentration of industrial activities, exacerbating air pollution in the region (Islam et al., 2020). The Kathmandu Valley's encirclement by high mountains makes it especially vulnerable to pollution. In contrast, Assam's plains are heavily influenced by the monsoon and high humidity, which promotes the diffusion and deposition of pollutants. Despite these regional differences, CO concentrations in these areas show strong correlations with levels in the Ali region, Nyingchi City, Shannan City, and Shigatse City on the Tibetan Plateau, with correlation coefficients (r) ranging from 0.52 to 0.71. These correlations suggest that long-distance pollutant transport, influenced by meteorological conditions such as monsoons, may link these regions to similar or shared pollution sources (Carrico et al., 2003).

The rapid increase in CO concentrations from South Asia, particularly India and Nepal, is closely linked to the rise in flux over the southwestern Tibetan Plateau, driven primarily by industrialization, agricultural activities, and population growth in the region. The topography of the Tibetan Plateau, combined with the monsoon system, facilitates the transport of pollutants from South Asia to the plateau. At the same time, the plateau's capacity to absorb CO plays a critical role in modulating regional fluxes. Furthermore, China’s domestic CO emissions have significantly decreased due to policy controls and economic restructuring. The Tibetan Plateau has long been regarded as an atmospheric background, with local anthropogenic emissions deemed negligible(Yao et al., 2012; Zheng et al., 2018; Kang et al., 2019; Sun et al., 2021). Overall, there is a dual trend of increasing external influx and decreasing internal efflux, with the concentration of CO received by the Tibetan Plateau from South Asia exceeding the influence of emissions from inland China.

4.3 Transboundary transport pathway

https://doi.org/10.5194/egusphere-2024-3252
Preprint. Discussion started: 6 December 2024

Spatial distribution of CO across four seasons around the Tibetan Plateau is shown in Figure 8, and Figure 9 presents the atmospheric circulation patterns at 200 hPa and 500 hPa, including mean horizontal wind vectors and latitude-height and longitude-height distributions. Significant seasonal variations in CO concentration are observed in the Tibetan Plateau and surrounding areas, primarily influenced by atmospheric circulation patterns, pollutant source strength, and deep convection activities. The interplay among these factors contributes to the complex dynamics of CO distribution, revealing the intricate relationship between local emissions and regional meteorological conditions.

The south Asian summer monsoon transports a substantial amount of air from the surface to the stratosphere, characterized by southwesterly winds in the lower troposphere and an anticyclonic circulation in the upper troposphere (Abe et al., 2013). This anticyclonic system, dominant in the upper troposphere and lower stratosphere, significantly affects CO distribution in the Tibetan Plateau by enhancing the transport of tropospheric pollutants into the stratosphere (Huang et al., 2023). The high-altitude terrain of the Tibetan Plateau amplifies this process, facilitating vertical lifting of air. Surface pollutants are transported to the upper troposphere through the Asian summer monsoon anticyclone and become confined within the South Asian High's anticyclonic system (Randel et al., 2010; Bian et al., 2012; Bian et al., 2020; Huang et al., 2023). This dynamic leads to a significant increase in CO concentration in the upper troposphere and lower stratosphere. During the summer monsoon season, the southwesterly monsoon winds carry substantial pollutants into the plateau, strongly influenced by intense deep convection. These winds uplift CO from the southern plateau and disperse it across the region (Fu et al., 2006). Large-scale deep convection plays a crucial role in lifting CO from upwind source regions to higher altitudes. While some CO returns to the source region, a portion is transported to the Tibetan Plateau by upper-level southwesterly winds.

In contrast, under dry winter monsoon conditions, CO can be transported to the Himalayan-Tibetan Plateau via the westerlies. The northwesterly flow rapidly conveys CO pollutants from the Northern Hemisphere to the Tibetan Plateau and its surrounding regions (Zhang et al., 2015; Sun et al., 2021). This winter flow typically introduces strong cold air, causing intense surface cooling upon entering the plateau and resulting in descending air currents. This process enhances local circulation, exacerbating CO accumulation (Liu et al., 2003; Zhang et al., 2015). Additionally, the plateau's topographical features influence CO distribution, as stable atmospheric stratification limits vertical dispersion, leading to accumulation in the lower troposphere.

However, the amount of CO transported to the plateau is also influenced by the location and intensity of sources, air mass trajectories, and transport timing (Yao et al., 2012; Zhang et al., 2015; Kang et al., 2019; Sun et al., 2021). Variations in CO concentration depend not only on seasonal atmospheric circulation patterns but also on the distribution and intensity of pollution sources and the frequency and strength of deep convection activity. These complex interactions lead to significant seasonal changes in CO concentrations.

5 Conclusions

In this study, we utilized data products of TROPOMI, ERA5, and GEOS-CF, along with the closed-loop integral method, to quantify transboundary transport flux of CO over the Tibetan

Plateau. The variabilities and driving forces of external influx, internal efflux, and net flux of CO over the closed-loop, southwestern, and northeastern segments of Tibetan Plateau were analyzed.

The closed-loop CO concentration along the Tibetan Plateau boundary shown significant spatiotemporal variations, with daily means ranging from 7.75×10^{17} to 15.61×10^{17} molec cm^{-2} and seasonal means from 10.06×10^{17} to 12.01×10^{17} molec cm^{-2}, and with high levels in the southeastern segment adjacent to southeastern Asia. The closed-loop, southwestern, and northeastern segments exhibit a bimodal cycle, peaking in late spring and early autumn, with significant autumn fluctuations and less variability in winter. During the South Asian monsoon, CO concentrations increased by 0.90×10^{17} molec cm^{-2} in the Tibetan Plateau, decreased by 1.78 $\times 10^{17}$ molec cm^{-2} in India, and decreased by 0.36×10^{17} molec cm^{-2} in Nepal compared to the annual average. A strong correlation and synchronization of CO concentrations were observed between the South Asian border region and the Tibetan Plateau. Over the past six years, CO total columns in Tibet, India, and Nepal exhibited growth trends of 0.54×10^{15} molec cm^{-2} yr^{-1}, 0.86×10^{15} molec cm^{-2} yr^{-1}, and 1.17×10^{15} molec cm^{-2} yr^{-1}, respectively. These trends are notably higher than the growth observed in Tibet. Over six years, growth trends of 0.68×10^{15} molec cm^{-2} yr^{-1}, 0.55×10^{15} molec cm^{-2} yr^{-1}, and 0.78×10^{15} molec cm^{-2} yr^{-1} were observed for each segment.

Transboundary transport flux of CO in the Tibetan Plateau is high in late autumn and winter, and low in summer. Six-year averaged external influx, internal efflux, and net flux are 17.70 t s^{-1} and 17.56 t s^{-1}, 0.13 t s^{-1}, respectively. The external influx shows a slight positive trend of 0.67 t s^{-1} yr^{-1}, while net flux increases at 1.07 t s^{-1} yr^{-1}, contrasted by a minor decline in internal efflux of -0.40 t s^{-1} yr^{-1}. In the southwestern segment, external influx and internal efflux show comparable variability, with annual means of 11.76 t s^{-1} and 4.41 t s^{-1}, and growth rates of 0.52 t s^{-1} yr^{-1} and -0.06 t s^{-1} yr^{-1}, respectively. Conversely, the northeastern segment exhibits significant differences, with average influx and efflux of 5.94 t s^{-1} and 13.17 t s^{-1}, and growth rates of 0.15 t s^{-1} yr^{-1} and -0.28 t s^{-1} yr^{-1}, respectively. In summary, these trends indicate an increase in external influx and a slight decrease in internal efflux across the Tibetan Plateau, with significant regional differences in CO fluxes; the southwestern segments serves as the primary contributor to external influx, exhibiting considerable seasonal changes, while the eastern segments shows lower external influx than internal efflux, indicating a net efflux.

We assessed the uncertainties of wind speed and direction across 22 layers from 1000 hPa to 50 hPa, obtaining average uncertainties of 3.39 m s^{-1} for wind speed and 54.55° for wind direction, with corrected averages of 0.78 m s^{-1} and 22.15°, respectively. The uncertainty in wind speed accounts for an average error of 6.99%, while the uncertainty in wind direction contributes an average error of 11.03%. The average error in CO total column along the Tibetan Plateau's closed-loop was 4.27%. Using the error propagation equation, the total uncertainty in CO flux from both factors is calculated to be 13.81%.

In conclusion, we quantified the CO flux over the Tibetan Plateau and found a significant seasonal trend, with an increasing external influx in recent years. Specifically, the southwestern segments of the Tibetan Plateau represent the primary source of CO, demonstrating an upward trend potentially associated with the rapid increase in CO concentrations from South Asia. Conversely, CO transmission to the eastern segments is declining, likely due to decreased emissions and the plateau's inherent capacity to absorb CO. The unique geographical position of the Tibetan Plateau makes it crucial for observing and investigating transboundary transport of

https://doi.org/10.5194/egusphere-2024-3252
Preprint. Discussion started: 6 December 2024

regional atmospheric pollutants, providing a scientific basis for understanding global pollutant transport mechanisms and informing environmental protection policies.

Data availability. The TROPOMI CO dataset of this study is available for download at https://scihub.copernicus.eu/ (last access: 16 June 2024). ERA5 hourly wind data are available download at https://cds.climate.copernicus.eu/ (last accessed: 1 June 2024). GEOS-CF simulations are available for download at https://gmao.gsfc.nasa.gov/ (last accessed: 12 April 2024). GEOS-Chem simulations in this study are available on request from Youwen Sun (ywsun@aiofm.ac.cn)

Author contributions. ZS carried out the data analysis and prepared the paper with input from all coauthors. YS designed the study. HY conducted the GEOS-Chem simulations and, along with XL, YS, ZP, CYL, and CL, provided constructive comments. HY also offered valuable insights into the data analysis.

Competing interests. The authors declare that they have no conflict of interest.

Acknowledgements. We thank the NASA Global Modeling and Assimilation Office (GMAO) for providing the GEOS-CF simulations, and the Copernicus Climate Change Service (C3S) for providing the ERA5 reanalysis data. We also express our gratitude to the GEOS-Chem team for sharing the model, and NOAA for providing the GEOS-FP meteorological files. Additionally, we thank the European Space Agency (ESA) for providing the Sentinel-5P TROPOMI CO data.

Financial support. This work is jointly supported by the National Science Fund for Excellent Young Scholars (No. 62322514, 62322513), National Science Foundation of China (12174367), Anhui Science Fund for Distinguished Young Scholars (No. 2308085J25) and National Key Research and Development Program of China (No. 2023YFC3709502).

References

Abe, M., Hori, M., Yasunari, T., and Kitoh, A.: Effects of the Tibetan Plateau on the onsetof the summer monsoon in South Asia: The role of the air-sea interaction, Journal of Geophysical Research: Atmospheres, 118, 1760-1776, 10.1002/jgrd.50210, 2013.

Assessment, A. C. I.: Impacts of a warming Arctic-Arctic climate impact assessment, 2004.

Bey, I., Jacob, D. J., Yantosca, R. M., Logan, J. A., Field, B. D., Fiore, A. M., Li, Q., Liu, H. Y., Mickley, L. J., and Schultz, M. G.: Global modeling of tropospheric chemistry with assimilated meteorology: Model description and evaluation, Journal of Geophysical Research: Atmospheres, 106, 23073-23095, 10.1029/2001jd000807, 2001.

Bian, J., Li, D., Bai, Z., Li, Q., Lyu, D., and Zhou, X.: Transport of Asian surface pollutants to the global stratosphere from the Tibetan Plateau region during the Asian summer monsoon, Natl Sci Rev, 7, 516-533, 10.1093/nsr/nwaa005, 2020.

Bian, J., Pan, L. L., Paulik, L., Vömel, H., Chen, H., and Lu, D.: In situ water vapor and ozone measurements in Lhasa and Kunming during the Asian summer monsoon, Geophysical Research Letters, 39, 10.1029/2012gl052996, 2012.

Bibi, S., Wang, L., Li, X., Zhou, J., Chen, D., and Yao, T.: Climatic and associated cryospheric, biospheric, and hydrological changes on the Tibetan Plateau: a review, International Journal of Climatology, 38, 10.1002/joc.5411, 2018.

Borsdorff, T., García Reynoso, A., Maldonado, G., Mar-Morales, B., Stremme, W., Grutter, M., and Landgraf, J.: Monitoring CO emissions of the metropolis Mexico City using TROPOMI CO observations, Atmospheric Chemistry and Physics, 20, 15761-15774, 10.5194/acp-20-15761-2020, 2020.

Carrico, C. M., Bergin, M. H., Shrestha, A. B., Dibb, J. E., Gomes, L., and Harris, J. M.: The importance of carbon and mineral dust to seasonal aerosol properties in the Nepal Himalaya, Atmospheric Environment, 37, 2811-2824, 10.1016/s1352-2310(03)00197-3, 2003.

Chen, F., Zhang, J., Liu, J., Cao, X., Hou, J., Zhu, L., Xu, X., Liu, X., Wang, M., Wu, D., Huang, L., Zeng, T., Zhang, S., Huang, W., Zhang, X., and Yang, K.: Climate change, vegetation history, and landscape responses on the Tibetan Plateau during the Holocene: A comprehensive review, Quaternary Science Reviews, 243, 10.1016/j.quascirev.2020.106444, 2020.

Cong, Z., Kang, S., Kawamura, K., Liu, B., Wan, X., Wang, Z., Gao, S., and Fu, P.: Carbonaceous aerosols on the south edge of the Tibetan Plateau: concentrations, seasonality and sources, Atmospheric Chemistry and Physics, 15, 1573-1584, 10.5194/acp-15-1573-2015, 2015.

Fu, R., Hu, Y., Wright, J. S., Jiang, J. H., Dickinson, R. E., Chen, M., Filipiak, M., Read, W. G., Waters, J. W., and Wu, D. L.: Short circuit of water vapor and polluted air to the global stratosphere by convective transport over the Tibetan Plateau, Proc Natl Acad Sci U S A, 103, 5664-5669, 10.1073/pnas.0601584103, 2006.

Gao, J., Yao, T., Masson-Delmotte, V., Steen-Larsen, H. C., and Wang, W.: Collapsing glaciers threaten Asia's water supplies, Nature, 565, 19-21, 10.1038/d41586-018-07838-4, 2019.

Gloudemans, A. M. S., Krol, M. C., Meirink, J. F., de Laat, A. T. J., van der Werf, G. R., Schrijver, H., van den Broek, M. M. P., and Aben, I.: Evidence for long-range transport of carbon monoxide in the Southern Hemisphere from SCIAMACHY observations, Geophysical Research Letters, 33, 10.1029/2006gl026804, 2006.

Heald, C. L., Jacob, D. J., Fiore, A. M., Emmons, L. K., Gille, J. C., Deeter, M. N., Warner, J., Edwards, D. P., Crawford, J. H., Hamlin, A. J., Sachse, G. W., Browell, E. V., Avery, M. A., Vay, S. A., Westberg, D. J., Blake, D. R., Singh, H. B., Sandholm, S. T., Talbot, R. W., and Fuelberg, H. E.: Asian outflow and trans-Pacific transport of carbon monoxide and ozone pollution: An integrated satellite, aircraft, and model perspective, Journal of Geophysical Research: Atmospheres, 108, 10.1029/2003jd003507, 2003.

Hersbach, H., Bell, B., Berrisford, P., Hirahara, S., Horányi, A., Muñoz-Sabater, J., Nicolas, J., Peubey, C., Radu, R., Schepers, D., Simmons, A., Soci, C., Abdalla, S., Abellan, X., Balsamo, G., Bechtold, P., Biavati, G., Bidlot, J., Bonavita, M., De Chiara, G., Dahlgren, P., Dee, D., Diamantakis, M., Dragani, R., Flemming, J., Forbes, R., Fuentes, M., Geer, A., Haimberger, L., Healy, S., Hogan, R. J., Hólm, E., Janisková, M., Keeley, S., Laloyaux, P., Lopez, P., Lupu, C., Radnoti, G., de Rosnay, P., Rozum, I., Vamborg, F., Villaume, S., and Thépaut, J. N.: The ERA5 global reanalysis, Quarterly Journal of the Royal Meteorological Society, 146, 1999-2049, 10.1002/qj.3803, 2020.

Holloway, T., Levy, H., and Kasibhatla, P.: Global distribution of carbon monoxide, Journal of Geophysical Research: Atmospheres, 105, 12123-12147, 10.1029/1999jd901173, 2000.

Huang, J., Zhou, X., Wu, G., Xu, X., Zhao, Q., Liu, Y., Duan, A., Xie, Y., Ma, Y., Zhao, P., Yang, S., Yang, K., Yang, H., Bian, J., Fu, Y., Ge, J., Liu, Y., Wu, Q., Yu, H., Wang, B., Bao, Q., and Qie, K.:

https://doi.org/10.5194/egusphere-2024-3252
Preprint. Discussion started: 6 December 2024

Global Climate Impacts of Land-Surface and Atmospheric Processes Over the Tibetan Plateau, Reviews of Geophysics, 61, 10.1029/2022rg000771, 2023.

Huang, Y., Li, A., Xie, P., Hu, Z., Xu, J., Fang, X., Ren, H., Li, X., and Dang, B.: NOx Emission Flux Measurements with Multiple Mobile-DOAS Instruments in Beijing, Remote Sensing, 12, 10.3390/rs12162527, 2020.

Hung, H., Halsall, C., Ball, H., Bidleman, T., Dachs, J., De Silva, A., Hermanson, M., Kallenborn, R., Muir, D., Suhring, R., Wang, X., and Wilson, S.: Climate change influence on the levels and trends of persistent organic pollutants (POPs) and chemicals of emerging Arctic concern (CEACs) in the Arctic physical environment - a review, Environ Sci Process Impacts, 24, 1577-1615, 10.1039/d1em00485a, 2022.

Islam, M. R., Jayarathne, T., Simpson, I. J., Werden, B., Maben, J., Gilbert, A., Praveen, P. S., Adhikari, S., Panday, A. K., Rupakheti, M., Blake, D. R., Yokelson, R. J., DeCarlo, P. F., Keene, W. C., and Stone, E. A.: Ambient air quality in the Kathmandu Valley, Nepal, during the pre-monsoon: concentrations and sources of particulate matter and trace gases, Atmospheric Chemistry and Physics, 20, 2927-2951, 10.5194/acp-20-2927-2020, 2020.

Jeong, U. and Hong, H.: Comparison of Total Column and Surface Mixing Ratio of Carbon Monoxide Derived from the TROPOMI/Sentinel-5 Precursor with In-Situ Measurements from Extensive Ground-Based Network over South Korea, Remote Sensing, 13, 10.3390/rs13193987, 2021.

Ji, Z., Kang, S., Cong, Z., Zhang, Q., and Yao, T.: Simulation of carbonaceous aerosols over the Third Pole and adjacent regions: distribution, transportation, deposition, and climatic effects, Climate Dynamics, 45, 2831-2846, 10.1007/s00382-015-2509-1, 2015.

Kang, S., Zhang, Q., Qian, Y., Ji, Z., Li, C., Cong, Z., Zhang, Y., Guo, J., Du, W., Huang, J., You, Q., Panday, A. K., Rupakheti, M., Chen, D., Gustafsson, O., Thiemens, M. H., and Qin, D.: Linking atmospheric pollution to cryospheric change in the Third Pole region: current progress and future prospects, Natl Sci Rev, 6, 796-809, 10.1093/nsr/nwz031, 2019.

Kaspari, S. D., Schwikowski, M., Gysel, M., Flanner, M. G., Kang, S., Hou, S., and Mayewski, P. A.: Recent increase in black carbon concentrations from a Mt. Everest ice core spanning 1860-2000 AD, Geophysical Research Letters, 38, n/a-n/a, 10.1029/2010gl046096, 2011.

Keller, C. A., Knowland, K. E., Duncan, B. N., Liu, J., Anderson, D. C., Das, S., Lucchesi, R. A., Lundgren, E. W., Nicely, J. M., Nielsen, E., Ott, L. E., Saunders, E., Strode, S. A., Wales, P. A., Jacob, D. J., and Pawson, S.: Description of the NASA GEOS Composition Forecast Modeling System GEOS-CF v1.0, J Adv Model Earth Syst, 13, e2020MS002413, 10.1029/2020MS002413, 2021.

Kunhikrishnan, T., Lawrence, M. G., von Kuhlmann, R., Richter, A., Ladstätter-Weißenmayer, A., and Burrows, J. P.: Analysis of tropospheric NOx over Asia using the model of atmospheric transport and chemistry (MATCH-MPIC) and GOME-satellite observations, Atmospheric Environment, 38, 581-596, 10.1016/j.atmosenv.2003.09.074, 2004.

Landgraf, J., Borsdorff, T., Langerock, B., and Keppens, A.: S5P mission performance centre carbon monoxide (L2 CO) readme, S5P-MPC-SRON-PRF-CO, 1.5, SRON Netherlands Institute for Space Research …, 2020.

Lawrence, M. G. and Lelieveld, J.: Atmospheric pollutant outflow from southern Asia: a review, Atmospheric Chemistry and Physics, 10, 11017-11096, 10.5194/acp-10-11017-2010, 2010.

https://doi.org/10.5194/egusphere-2024-3252
Preprint. Discussion started: 6 December 2024

Lee, H. M. and Park, R. J.: Factors determining the seasonal variation of ozone air quality in South Korea: Regional background versus domestic emission contributions, Environ Pollut, 308, 119645, 10.1016/j.envpol.2022.119645, 2022.

Leguijt, G., Maasakkers, J. D., Denier van der Gon, H. A. C., Segers, A. J., Borsdorff, T., and Aben, I.: Quantification of carbon monoxide emissions from African cities using TROPOMI, Atmospheric Chemistry and Physics, 23, 8899-8919, 10.5194/acp-23-8899-2023, 2023.

Li, C., Su, F., Yang, D., Tong, K., Meng, F., and Kan, B.: Spatiotemporal variation of snow cover over the Tibetan Plateau based on MODIS snow product, 2001–2014, International Journal of Climatology, 38, 708-728, 10.1002/joc.5204, 2017.

Li, C., Yan, F., Kang, S., Yan, C., Hu, Z., Chen, P., Gao, S., Zhang, C., He, C., Kaspari, S., and Stubbins, A.: Carbonaceous matter in the atmosphere and glaciers of the Himalayas and the Tibetan plateau: An investigative review, Environ Int, 146, 106281, 10.1016/j.envint.2020.106281, 2021.

Liu, H., Jacob, D. J., Bey, I., Yantosca, R. M., Duncan, B. N., and Sachse, G. W.: Transport pathways for Asian pollution outflow over the Pacific: Interannual and seasonal variations, Journal of Geophysical Research: Atmospheres, 108, 10.1029/2002jd003102, 2003.

Long, M. S., Yantosca, R., Nielsen, J. E., Keller, C. A., da Silva, A., Sulprizio, M. P., Pawson, S., and Jacob, D. J.: Development of a grid-independent GEOS-Chem chemical transport model (v9-02) as an atmospheric chemistry module for Earth system models, Geoscientific Model Development, 8, 595-602, 10.5194/gmd-8-595-2015, 2015.

Luo, M., Read, W., Kulawik, S., Worden, J., Livesey, N., Bowman, K., and Herman, R.: Carbon monoxide (CO) vertical profiles derived from joined TES and MLS measurements, Journal of Geophysical Research: Atmospheres, 118, 10.1002/jgrd.50800, 2013.

Lüthi, Z. L., Škerlak, B., Kim, S. W., Lauer, A., Mues, A., Rupakheti, M., and Kang, S.: Atmospheric brown clouds reach the Tibetan Plateau by crossing the Himalayas, Atmospheric Chemistry and Physics, 15, 6007-6021, 10.5194/acp-15-6007-2015, 2015.

Martínez-Alonso, S., Deeter, M., Worden, H., Borsdorff, T., Aben, I., Commane, R., Daube, B., Francis, G., George, M., Landgraf, J., Mao, D., McKain, K., and Wofsy, S.: 1.5 years of TROPOMI CO measurements: comparisons to MOPITT and ATom, Atmospheric Measurement Techniques, 13, 4841-4864, 10.5194/amt-13-4841-2020, 2020.

Qian, Y., Flanner, M. G., Leung, L. R., and Wang, W.: Sensitivity studies on the impacts of Tibetan Plateau snowpack pollution on the Asian hydrological cycle and monsoon climate, Atmospheric Chemistry and Physics, 11, 1929-1948, 10.5194/acp-11-1929-2011, 2011.

Ramanathan, V., Chung, C., Kim, D., Bettge, T., Buja, L., Kiehl, J. T., Washington, W. M., Fu, Q., Sikka, D. R., and Wild, M.: Atmospheric brown clouds: impacts on South Asian climate and hydrological cycle, Proc Natl Acad Sci U S A, 102, 5326-5333, 10.1073/pnas.0500656102, 2005.

Randel, W. J., Park, M., Emmons, L., Kinnison, D., Bernath, P., Walker, K. A., Boone, C., and Pumphrey, H.: Asian monsoon transport of pollution to the stratosphere, Science, 328, 611-613, 10.1126/science.1182274, 2010.

Shaiganfar, R., Beirle, S., Sharma, M., Chauhan, A., Singh, R. P., and Wagner, T.: Estimation of NO_x emissions from Delhi using Car MAX-DOAS observations and comparison with OMI satellite data, Atmospheric Chemistry and Physics, 11, 10871-10887, 10.5194/acp-11-10871-2011, 2011.

Shaiganfar, R., Beirle, S., Denier van der Gon, H., Jonkers, S., Kuenen, J., Petetin, H., Zhang, Q., Beekmann, M., and Wagner, T.: Estimation of the Paris

https://doi.org/10.5194/egusphere-2024-3252
Preprint. Discussion started: 6 December 2024

NO_{<i>x</i>} emissions from mobile MAX-DOAS observations and CHIMERE model simulations during the MEGAPOLI campaign using the closed integral method, Atmospheric Chemistry and Physics, 17, 7853-7890, 10.5194/acp-17-7853-2017, 2017.

Sheng, J., Wang, X., Gong, P., Joswiak, D. R., Tian, L., Yao, T., and Jones, K. C.: Monsoon-driven transport of organochlorine pesticides and polychlorinated biphenyls to the Tibetan Plateau: three year atmospheric monitoring study, Environ Sci Technol, 47, 3199-3208, 10.1021/es305201s, 2013.

Sun, Y., Yin , H., Cheng, Y., Zhang, Q., Zheng, B., Notholt, J., Lu, X., Liu, C., Tian, Y., and Liu, J.: Quantifying variability, source, and transport of CO in the urban areas over the Himalayas and Tibetan Plateau, Atmospheric Chemistry and Physics, 21, 9201-9222, 10.5194/acp-21-9201-2021, 2021.

Tan, W., Zhao, S., Liu, C., Chan, K. L., Xie, Z., Zhu, Y., Su, W., Zhang, C., Liu, H., Xing, C., and Liu, J.: Estimation of winter time NOx emissions in Hefei, a typical inland city of China, using mobile MAX-DOAS observations, Atmospheric Environment, 200, 228-242, 10.1016/j.atmosenv.2018.12.009, 2019.

Veefkind, J. P., Aben, I., McMullan, K., Förster, H., de Vries, J., Otter, G., Claas, J., Eskes, H. J., de Haan, J. F., Kleipool, Q., van Weele, M., Hasekamp, O., Hoogeveen, R., Landgraf, J., Snel, R., Tol, P., Ingmann, P., Voors, R., Kruizinga, B., Vink, R., Visser, H., and Levelt, P. F.: TROPOMI on the ESA Sentinel-5 Precursor: A GMES mission for global observations of the atmospheric composition for climate, air quality and ozone layer applications, Remote Sensing of Environment, 120, 70-83, 10.1016/j.rse.2011.09.027, 2012.

Wang, X., Zhang, Q., Zhang, Y., Cong, Z., Xu, B., Ji, Z., and Kang, S.: The transboundary transport of air pollutants and their environmental impacts on Tibetan Plateau, Chinese Science Bulletin, 64, 2876-2884, 10.1360/tb-2019-0135, 2019.

Wu, G., Wan, X., Ram, K., Li, P., Liu, B., Yin, Y., Fu, P., Loewen, M., Gao, S., Kang, S., Kawamura, K., Wang, Y., and Cong, Z.: Light absorption, fluorescence properties and sources of brown carbon aerosols in the Southeast Tibetan Plateau, Environ Pollut, 257, 113616, 10.1016/j.envpol.2019.113616, 2020.

Xu, B., Cao, J., Hansen, J., Yao, T., Joswia, D. R., Wang, N., Wu, G., Wang, M., Zhao, H., Yang, W., Liu, X., and He, J.: Black soot and the survival of Tibetan glaciers, Proc Natl Acad Sci U S A, 106, 22114-22118, 10.1073/pnas.0910444106, 2009.

Xu, Y., Su, W., Hu, Q., Zhang, C., Javed, Z., Tian, Y., Hou, H., and Liu, C.: Unexpected HCHO transnational transport: influence on the temporal and spatial distribution of HCHO in Tibet from 2013 to 2021 based on satellite, npj Climate and Atmospheric Science, 7, 10.1038/s41612-024-00639-9, 2024.

Yan, R. and Bian, J.: Tracing the boundary layer sources of carbon monoxide in the Asian summer monsoon anticyclone using WRF-Chem, Advances in Atmospheric Sciences, 32, 943-951, 10.1007/s00376-014-4130-3, 2015.

Yang, K., Koike, T., Fujii, H., Tamura, T., Xu, X., Bian, L., and Zhou, M.: The Daytime Evolution of the Atmospheric Boundary Layer and Convection over the Tibetan Plateau: Observations and Simulations, Journal of the Meteorological Society of Japan. Ser. II, 82, 1777-1792, 10.2151/jmsj.82.1777, 2004.

Yao, T., Thompson, L., Yang, W., Yu, W., Gao, Y., Guo, X., Yang, X., Duan, K., Zhao, H., Xu, B., Pu, J., Lu, A., Xiang, Y., Kattel, D. B., and Joswiak, D.: Different glacier status with atmospheric circulations in Tibetan Plateau and surroundings, Nature Climate Change, 2, 663-667, 10.1038/nclimate1580, 2012.

Yin, H., Sun, Y., Notholt, J., Palm, M., Ye, C., and Liu, C.: Quantifying the drivers of surface ozone anomalies in the urban areas over the Qinghai-Tibet Plateau, Atmospheric Chemistry and Physics, 22, 14401-14419, 10.5194/acp-22-14401-2022, 2022.

Yu, P., Rosenlof, K. H., Liu, S., Telg, H., Thornberry, T. D., Rollins, A. W., Portmann, R. W., Bai, Z., Ray, E. A., Duan, Y., Pan, L. L., Toon, O. B., Bian, J., and Gao, R. S.: Efficient transport of tropospheric aerosol into the stratosphere via the Asian summer monsoon anticyclone, Proc Natl Acad Sci U S A, 114, 6972-6977, 10.1073/pnas.1701170114, 2017.

Zhang, M., Zhao, C., Cong, Z., Du, Q., Xu, M., Chen, Y., Chen, M., Li, R., Fu, Y., Zhong, L., Kang, S., Zhao, D., and Yang, Y.: Impact of topography on black carbon transport to the southern Tibetan Plateau during the pre-monsoon season and its climatic implication, Atmospheric Chemistry and Physics, 20, 5923-5943, 10.5194/acp-20-5923-2020, 2020.

Zhang, R., Wang, H., Qian, Y., Rasch, P. J., Easter, R. C., Ma, P. L., Singh, B., Huang, J., and Fu, Q.: Quantifying sources, transport, deposition, and radiative forcing of black carbon over the Himalayas and Tibetan Plateau, Atmospheric Chemistry and Physics, 15, 6205-6223, 10.5194/acp-15-6205-2015, 2015.

Zheng, B., Tong, D., Li, M., Liu, F., Hong, C., Geng, G., Li, H., Li, X., Peng, L., Qi, J., Yan, L., Zhang, Y., Zhao, H., Zheng, Y., He, K., and Zhang, Q.: Trends in China's anthropogenic emissions since 2010 as the consequence of clean air actions, Atmospheric Chemistry and Physics, 18, 14095-14111, 10.5194/acp-18-14095-2018, 2018.

Figures

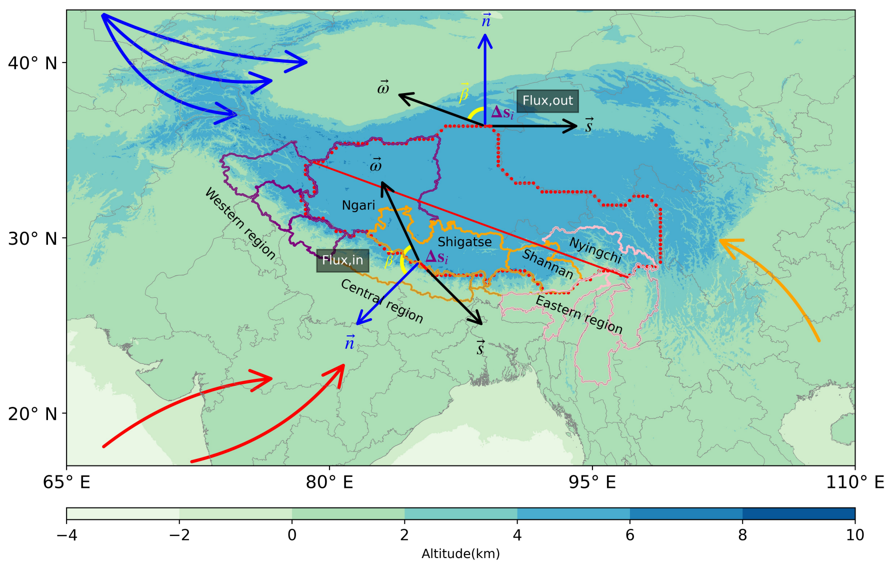

Fig. 1. Geographical description of the Tibetan Plateau and demonstration of the closed-loop integral method for CO flux calculation, with red points indicating the closed-loop. Surrounding areas are categorized into western (in

https://doi.org/10.5194/egusphere-2024-3252
Preprint. Discussion started: 6 December 2024

purple), central (in orange), and eastern (in pink) regions. Within the Tibetan Plateau, highlighted areas include Ngari Prefecture, Shigatse City, Shannan City, and Nyingchi City. Elevation data is sourced from NOAA NCEI. The red bold line split the closed-loop of the Tibetan Plateau into southeastern and northeastern segments.

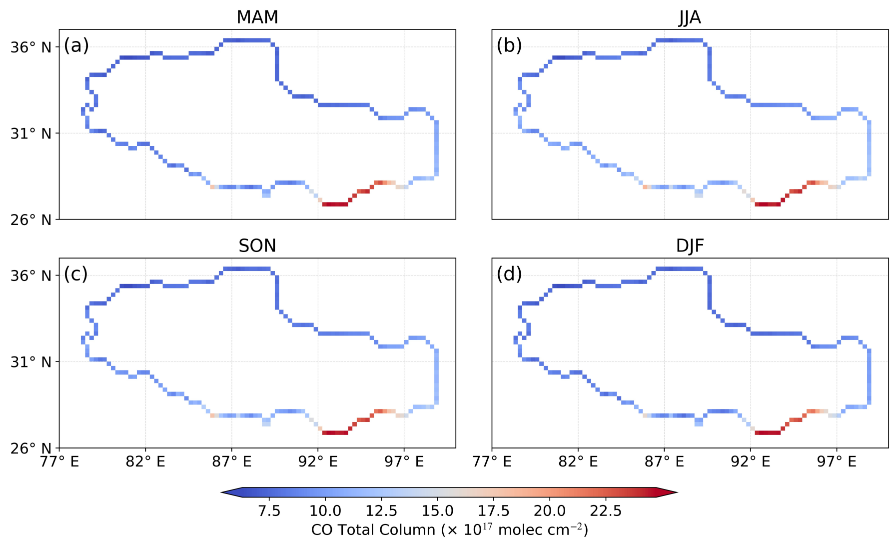

Fig. 2. Seasonal average of CO total column over the Tibetan Plateau, which is derived from data collected across all days from May 2018 to April 2024, and is categorized by spring, summer, autumn, and winter.

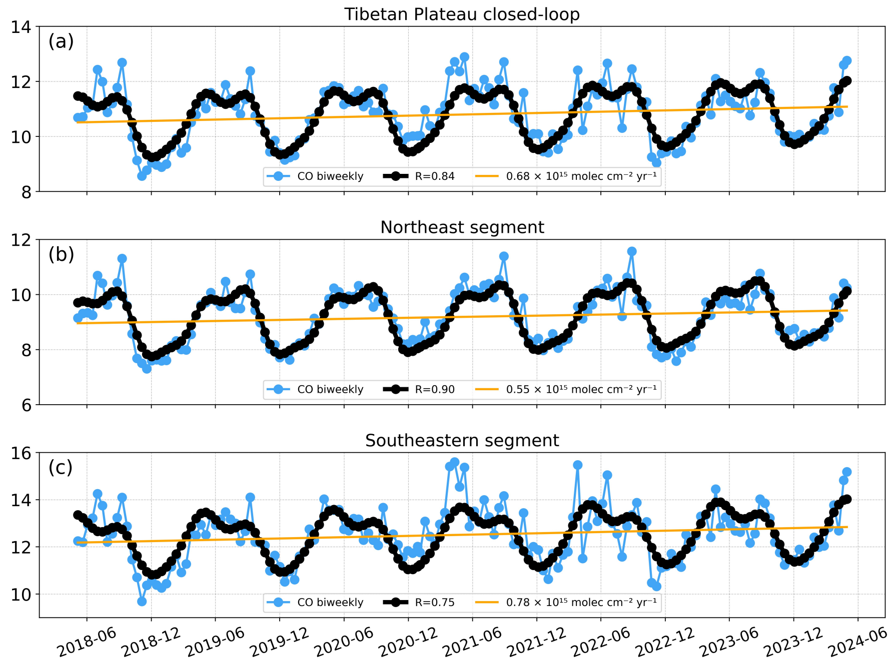

Fig. 3. Panels (a), (b), and (c) depict the inter-annual variabilities of CO concentrations in the closed-loop of the

https://doi.org/10.5194/egusphere-2024-3252
Preprint. Discussion started: 6 December 2024

Tibetan Plateau, as well as the northeastern and southwestern segments, from May 2018 to April 2024. Blue dots represent biweekly averaged CO total column. The figures illustrate the seasonal trend (black line) and inter-annual trend (orange line) fitted by the seasonal cycle model.

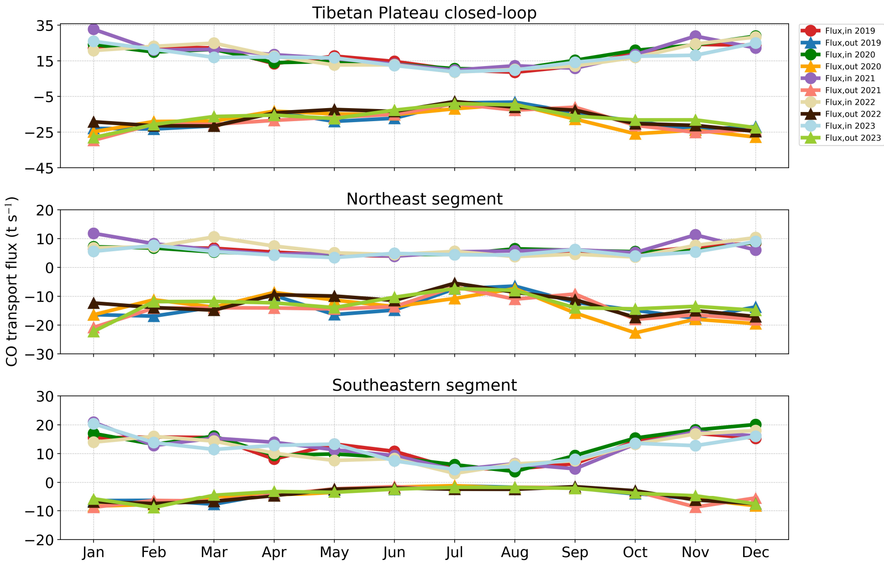

Fig. 4. Monthly averaged external influx and internal efflux of CO over the closed-loop, the southwestern, and the northeastern segments of the Tibetan Plateau. Results are presented based on five complete years (2019–2023).

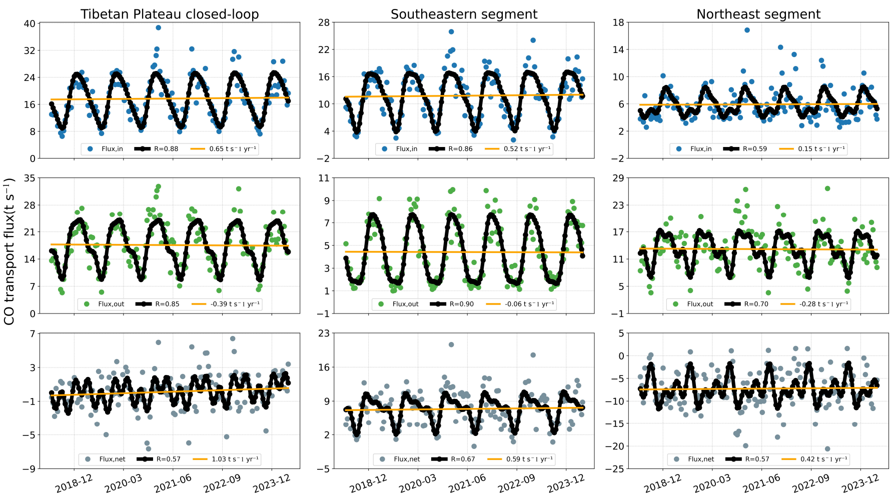

Fig. 5. Inter-annual variabilities of external influx, internal efflux and net flux of CO over the closed-loop, the southwestern, and the northeastern segments of the Tibetan Plateau from May 2018 to April 2024. Blue dots represent external influx, green dots indicate internal efflux, and gray dots show net flux. The seasonal trend (black line) and inter-annual trend (orange line) are fitted using the seasonal cycle model.

https://doi.org/10.5194/egusphere-2024-3252
Preprint. Discussion started: 6 December 2024

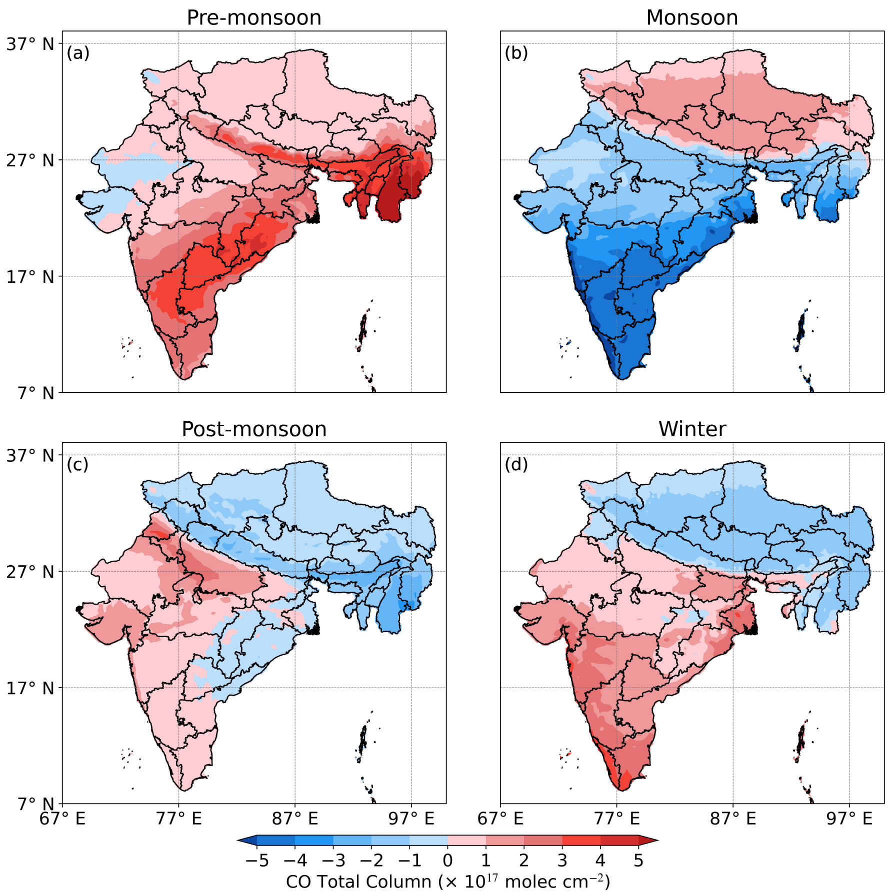

Fig. 6. CO total columns over the Tibetan Plateau and south Asia during the pre-monsoon, monsoon, post-monsoon, and winter. The data are collected from May 2018 to April 2024.

https://doi.org/10.5194/egusphere-2024-3252
Preprint. Discussion started: 6 December 2024

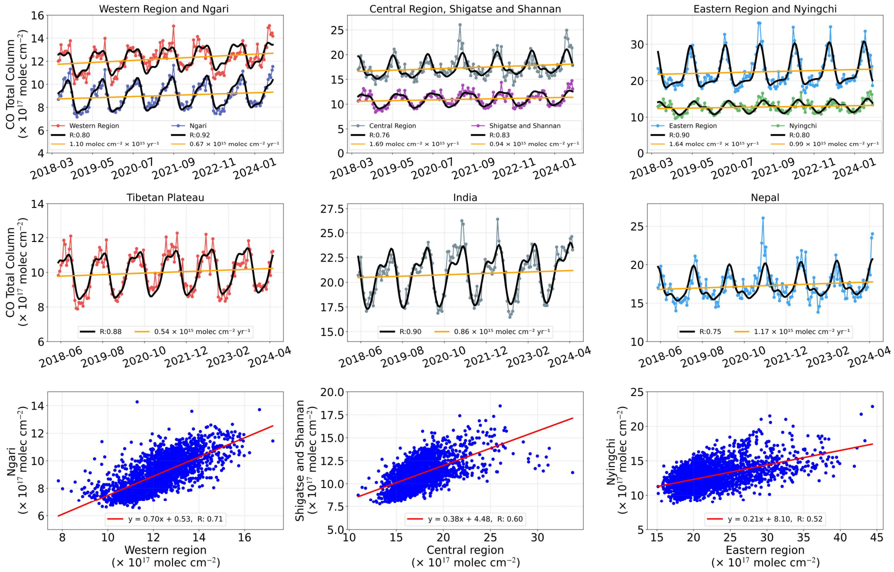

Fig. 7. Seasonal, inter-annual variabilities, and correlation analysis of CO concentrations over the western, central, and eastern regions outside the Tibetan Plateau, and over the Ngari, Shigatse, Shannan, and Nyingchi within the Tibetan Plateau. The red, dark blue, gray, purple, blue, and green dots in the figure represent CO concentrations in the western region outside the Tibetan Plateau, Ngari, the central region outside the Tibetan Plateau, Shigatse, Shannan, the eastern region outside the Tibetan Plateau, and Nyingchi, respectively.

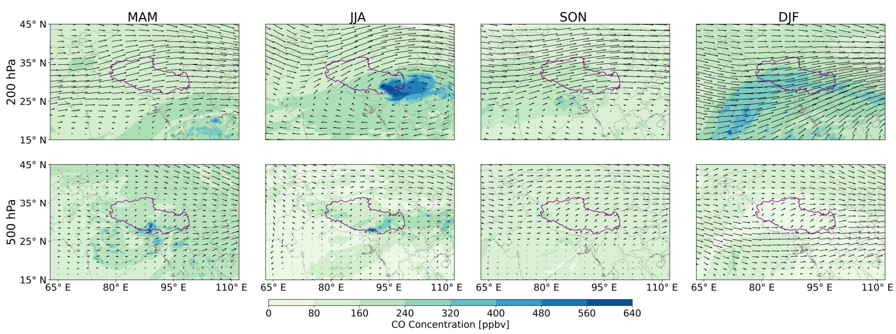

Fig. 8. Spatial distribution of CO concentration surrounding the Tibetan Plateau across different seasons, alongside mean horizontal wind vectors at 200 hPa and 500 hPa, represented by arrows. The study area is outlined in purple. The CO spatial distribution data is available from GEOS-CF, while the meteorological fields are derived from ERA5.

https://doi.org/10.5194/egusphere-2024-3252
Preprint. Discussion started: 6 December 2024

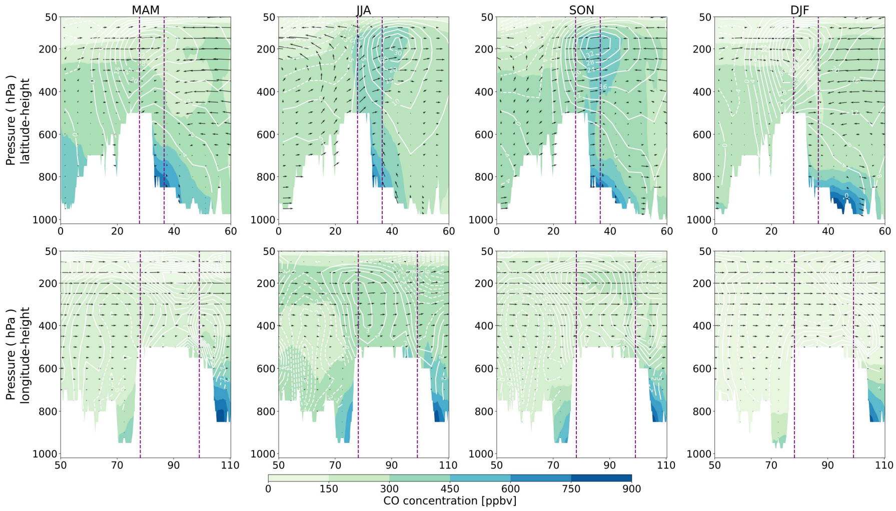

Fig. 9. The first row shows the latitudinal–altitude distribution of CO concentrations in different seasons averaged over the range 50°–110° E (positions correspond to different columns). The white contours at intervals of 18 m $^{s-1}$ represent the westerly (solid) and easterly (dashed) mean meridional winds; the white areas represent the terrain, and the arrows represent the wind vectors (vertical speed units are 10^{-4} hPa s^{-1}, zonal wind units are m s^{-1}); the study area is marked by the purple dashed line. The second row is calculated from the longitude–altitude angles, averaged over the range 27°–33°N. Here the white contours represent the southerly (solid) and northerly (dashed) mean zonal winds, and the horizontal component of the wind vector is the meridional wind (m s^{-1}). The meteorological fields are from ERA5.

https://doi.org/10.5194/egusphere-2024-3252
Preprint. Discussion started: 6 December 2024

Tables

Table 1. Statistics of the external influx and internal efflux of CO across the closed-loop, the southwestern and northeastern segments of the Tibetan Plateau from May 2018 to April 2024.

Type / Year			2018	2019	2020	2021	2022	2023	2024
Seasonal cycle (monthly mean)	Tibetan	Flux,in max/min (t/s)	22.69/7.90 (12/8)	24.21/8.54 (11/8)	28.88/10.24 (12/8)	32.73/9.77 (1/7)	28.33/8.69 (12/7)	25.95/8.88 (1/7)	23.12/18.40 (3/4)
		Flux,out max/min (t/s)	22.45/7.89 （12/8）	23.56/8.16 (11/8)	27.80/9.37 (12/8)	29.61/9.10 (1/7)	24.61/7.84 (12/7)	28.08/9.05 (1/7)	22.18/16.65 (3/1)
	southwestern segment	Flux,in max/min (t/s)	15.21/3.57 (12/8)	17.04/4.66 (11/8)	20.09/3.77 12/8	20.89/4.35 (1/7)	17.98/3.12 (12/7)	20.36/4.48 (1/7)	16.69/11.10 (3/1)
		Flux,out max/min (t/s)	7.18/1.25 (11/7)	8.21/1.19 (12/7)	8.41/1.15 (1/7)	8.79/1.47 (1/6)	7.56/1.49 (12/9)	8.86/1.71 (2/7)	7.14/5.89 (1/3)
	northeastern segment	Flux,in max/min (t/s)	7.89/3.71 (11/10)	8.48/3.88 (12/6)	8.79/4.46 (12/7)	11.84/3.85 (1/6)	10.59/3.63 (3/10)	9.01/3.42 (12/5)	6.80/4.33 (1/4)
		Flux,out max/min (t/s)	15.97/5.84 (12/8)	17.63/6.47 (11/8)	22.69/7.35 (10/8)	20.82/6.73 (1/7)	17.34/5.47 (10/7)	22.21/7.34 (1/7)	16.30/9.52 (3/1)

Table 2. Uncertainties in the corrected mean wind speed and direction for the wind field used for calculating the closed-loop flux of CO over the Tibetan Plateau.

Year	Averaged Wind Speed Uncertainty (m/s)				Averaged Wind Direction and Its Uncertainty (°)			
	MAM	JJA	SON	DJF	MAM	JJA	SON	DJF
2018	0.78	1.15	0.60	0.67	22.31	34.09	18.10	19.07
2019	0.65	0.92	0.60	0.71	19.84	24.90	18.23	23.91
2020	0.75	0.93	0.53	0.65	23.19	24.17	13.99	22.69
2021	0.70	1.03	0.65	0.67	18.10	28.24	20.62	21.23
2022	0.84	0.90	0.59	0.68	26.41	28.05	16.50	20.02
2023	0.67	1.07	0.65	0.68	18.65	31.01	19.53	22.28
2024	0.66	-	-	-	19.41	-	-	-